Effect of Technological Mismatch on Photovoltaic Array: Analysis of Relative Power Loss

Stephen Ndubuisi Nnamchi [a*], Onyinyechi Adanma Nnamchi [b], Kevin Nnanye Nwaigwe [c], Zaid Oluwadurotimi Jagun [d], Johnson Ugochukwu Ezenwankwo [a]

[a] Department of Mechanical Engineering, School of Engineering and Applied Sciences, Kampala International University, P. O. Box: 20000 Ggaba, Kansanga, Kampala, Uganda.
[b] Department of Agricultural Engineering and Bio Resources, Michael Okpara University of Agriculture, Umudike, Umuahia, Nigeria.
[c] Department of Mechanical Engineering, Faculty of Engineering and Technology, University of Botswana, Gaborone, Botswana.
[d] Department of Computer Engineering, Olabisi Onabanjo University, Ibogun, Nigeria.

ABSTRACT

This study conducts a comparative evaluation of the performance of modules and the arrays under standard test conditions. An equivalent circuit model was developed alongside a computational scheme. The model input data were obtained from the manufacturer's specification datasheets. They were used to analyse the maximum Fill Factor (FF) and Relative Power Losses (RPL) for Parallel (P), Series (S) and Series-Parallel (SP) configurations. For matching modules, the RPL was insignificant, but for mismatched modules, the parallel configuration (P) and series-parallel (SP) yielded RPL of 1.3 %, while the series configuration (S) produced RPL of 2.6 %. Thus, short circuit defects associated with the P and SP configuration were well below the open circuit defects associated with the series configuration (S). These results clearly show that the large photovoltaic plant needs to be configured with multiple blocks or strings of SP configuration in order to suppress RPL. In addition, the designer and installers of large solar power plants should adopt modules with uniform electrical and thermal properties in the construction of large solar power plants. The trivial RPL associated with the matched modules should be taken into consideration, as well.

1. INTRODUCTION

A paradigm shift from brown to green energy aims to preserve our environment and provide a cost-effective and sustainable energy supply to meet the domestic and industrial energy demands of our society. This quest fosters extensive research on the optimization of energy generated from different renewable energy sources, irrespective of natural constraints and adversities which pose challenges to the exploitation of energy from renewable resources, particularly in solar energy resources [1, 2]. The simplest device employed in the conversion of solar energy into electricity (by helio-photovoltaic process) is commonly known as photovoltaic device. Photovoltaic device consists of cells in the decreasing order of efficiency: monocrystalline, polycrystalline and amorphous silicon and thin film cells [3, 4]. These cells are the building blocks of the modules, while aggregating the module forms an array.

The factors militating against the conversion of solar energy into domestic and industrial power could be attributed to asymmetry in manufacturing, degradation of module blossoming surface, manufacturing defects, broken cells,

snow, dirt (or soil) on the anterior part of the modules, aging of the materials used in encapsulation of the cells, uneven radiation of the modules, tilt, orientation, stringing configuration, and shading of modules and arrays [5, 6]. These challenges are responsible for power losses within modules and arrays. Losses may be attributed to an imbalance in the output power of the modules relative to the sum of the output power of the individual cells making up the modules. This phenomenon is commonly known as a mismatch effect of photovoltaic devices. This phenomenon is due to some cells not generating the expected optimum output power in the arrays [7]. The presence of the aforementioned challenges for the photovoltaic device engenders multiple peak powers, which make the probability of the photovoltaic system operating at global peak power null in the absence of Maximum Power Point Tracking (MPPT) or power electronics devices. Although shading solar cells do not have a significant effect on parallel configurations, recent works on optimization of the output power have suggested that parallel system configuration with a fully installed DC-DC converter and micro-inverter on the individual modules boosted the voltage supply for the standalone and grid connected systems, respectively [4, 8]. In series configuration, the individual module has to be installed with MPPT or bypass diode in order to exploit enough power from the series configuration.

*Corresponding Author's Email: stephen.nnamchi@kiu.ac.ug (S.N. Nnamchi)
URL: https://www.jree.ir/article_137215.html

Otherwise, failure or defect of one of the cells could be catastrophic in the generation of power, leading to hotspot, which impairs the efficiency of the semi-conductor materials in the photovoltaic modules, causing the disappearance of the junction that drives the charge carriers round the circuit [9].

Reconfiguration of the photovoltaic system has been discovered to be an effective means of achieving significant power harvest from photovoltaic devices [10]. Techniques for reconfiguring photovoltaic system include Total-Cross-Tied (TCT) technique, Bridge-Linked (BL) approach, Honeycomb (HC) method, Ladder Interconnection (LAD) technique, and the Su Do Ku logical pattern [11]. Reconfiguring the photovoltaic system is aimed at increasing the output power from the photovoltaic modules arranged in series-parallel configuration. Notwithstanding, the cost of the auxiliary installation and increment in output power ranging from 4.1-10 % [12] ought to be balanced. However, increasing the components of most engineering systems tend to increase the capital cost of the system and subsequently decrease the efficiency of the system. Introducing more linking wires by the virtue of reconfiguring the photovoltaic device may cause a greater voltage drop in the wires, which could affect the output power negatively while sustaining the output current from being cut off or diminished. Thus, parallel configuration requires a thick wire to carry current to the converter within a limited distance not beyond 3.408 m, while the series connection requires a thin wire that has the capacity to carry generated current beyond a distance of over 34.08 m [13]. The demerits of low-output current and voltage discredits a purely series and parallel configuration in the absence of the current and voltage ancillaries, respectively. However, series-parallel configuration has the potential to boost the output power even in the phase of shadings [14].

Most of the findings on the best technique for the reconfiguring photovoltaic device were based on the simulated results in different Nominal Operating Conditions (NOC), Nominal Operating Cell Temperature (NOCT), or PVUSA Test Condition (PTC). This approach is challenged by unevenly distributed global irradiance. Moreover, some of the cells may be under the nominal operating condition. Thus, there is a salient need to consider standard test condition, STC, which is not susceptible to most of these problems enumerated above while carrying out the performance analysis of different modules and array configuration. Research works [15, 16] support that at STC, Air Mass (AM) of 1.5 gives the best distribution of the spectrum and invariably uniform distribution of irradiance on the modules and arrays. The STC data from the manufacturer's sheet are equivalent to the measured or experimental data. This power is the output of the cells making up a module. Besides, an ideal or conventional model describing the behavior of the photovoltaic device is not configurationally suitable for generating the current-voltage (I-V) curves and power-voltage (P-V) curves because the number of series and parallel modules is not incorporated in this model. Thus, a modified model that integrates the number of series and parallel modules has to be employed for the purpose of generating I-V and P-V characteristic curves, which truly unveils the performance characteristics of different modules and array configurations [17, 18]. It is generally asserted that series resistance increases the output voltage, while parallel resistance increases the output current of modules and arrays. In the same vein, series configuration increases the output

voltage, whereas parallel configuration increases the output current [19].

The resulting effect of hybridizing both the series and parallel configurations deserves a general verification and proof, which is the main driver of the present work. Besides, the current work tends to show additional inherent mismatch (variation in electrical and thermal properties of the semiconductors) emanating from the erroneous configuration of an array with the modules of different number of cells (known as technological mismatch), which causes Relative Power Losses (RPL) above 3 % against the common mismatch [6], which is known to cause RPL between 0.53-3 % [20]. The RPL is based on the difference between the fill factor of cells and that of the module.

Thus, the present work is aimed at showing module or array configuration that is least susceptible to technological mismatch or most efficient configuration by considering the performance curves of the series, parallel and series-parallel configuration for the modules or array with a uniform (homogeneous) and non-uniform (heterogeneous) electrical and thermal characteristics.

2. THE EQUIVALENT CIRCUIT MODEL

The equivalent circuit model that depicts the helio-photovoltaic phenomenon is diagrammatically represented in Figures 1a-1c. In accordance with Kirchhoff's nodal law, the output current in the equivalent circuit model in non-standard test conditions is modeled as follows [21, 22]:

$$
\begin{aligned}
I = n_p I_{ph} &- n_p I_D - n_p I_p \\
&= n_p I_{ph} \\
&- n_p I_0 \left(\exp\left(\frac{\frac{V}{n_s} + \frac{IR_s}{n_p}}{n_p A V_T} \right) - 1 \right) \\
&- n_p \frac{\frac{V}{n_s} + \frac{IR_s}{n_p}}{R_p}
\end{aligned}
$$

or   (1)

$$
\begin{aligned}
I = n_p I_{ph} &- n_p I_D - n_p I_p \\
&= n_p I_{ph} \\
&- n_p I_0 \left(\exp\left(\frac{\frac{n_p V}{n_s} + IR_s}{n_p A V_T} \right) - 1 \right) \\
&- \frac{\frac{n_p V}{n_s} + IR_s}{R_p}
\end{aligned}
$$

However, the output current in the equivalent circuit in the standard test condition (0) is modeled as follows:

$$
\begin{aligned}
I = n_p I_{ph\_0} &- n_p I_{D\_0} - n_p I_{p\_0} \\
&= n_p I_{ph\_0} \\
&- n_p I_{0\_0} \left(\exp\left(\frac{\frac{n_p V}{n_s} + IR_{s\_0}}{n_p A_0 V_T} \right) - 1 \right) \\
&- \frac{\frac{n_p V}{n_s} + IR_{s\_0}}{R_{p\_0}}
\end{aligned}
$$
(2)

where A = ideality factor ($1 \leq A \leq 2$ [23, 24]), I = the output current (A), I_D = diode current (A), I_0 = diode reverse or saturation current (A), I_p = shunt current (A), I_{ph} = photon current (A), n_p = number of parallel modules (-), n_s = number

of series modules (-), R_p = shunt or parallel resistance (Ω), R_s = series resistance (Ω), V= the output voltage (V) and V_T = thermal voltage (V).

The model and nodal analysis of the Helio-photovoltaic circuit is made feasible by considering the three important standard conditions [25]: the short circuit, SC (in standard condition, 1), the maximum power point, mpp (in standard condition, 2), and open circuit, OC (3) in standard condition 1 ($I = I_{sc}$, V = 0), standard condition 2 ($I = I_{mpp}$, $V = V_{mpp}$), and standard condition 3 ($I = 0$, $V = V_{oc}$).

These standard conditions are imposed on Equation (2) to obtain the following three standard analytical equations:

For standard condition, 1 ($I = I_{sc}$, V = 0):

$$I_{sc} = n_p I_{ph\_0} - n_p I_{0\_0} \left(\exp\left(\frac{I_{sc} R_{s\_0}}{n_p A_0 V_T} \right) - 1 \right) - \frac{I_{sc} R_{s\_0}}{R_{p\_0}}$$

(3)

For $R_{s\_0} = 0$, Equation (3) becomes:

$$n_p I_{ph\_0} = I_{sc}$$

(4)

For standard condition, 2 ($I = I_{mpp}$, $V = V_{mpp}$):

$$I_{mpp} = n_p I_{ph\_0} - n_p I_{0\_0} \left(\exp\left(\frac{\frac{n_p V_{mpp}}{n_s} + I_{mpp} R_{s\_0}}{n_p A_0 V_T} \right) - 1 \right) - \frac{\frac{n_p V_{mpp}}{n_s} + I_{mpp} R_{s\_0}}{R_{p\_0}}$$

(5)

For standard condition, 3 ($I = 0$, $V = V_{oc}$):

$$0 = n_p I_{ph\_0} - n_p I_{0\_0} \left(\exp\left(\frac{\frac{n_p V_{oc}}{n_s}}{n_p A_0 V_T} \right) - 1 \right) - \frac{\frac{n_p V_{oc}}{n_s}}{R_{p\_0}}$$

(6)

, respectively.

Equation (3) can be re-written as follows:

$$n_p I_{ph\_0} = n_p I_{sc} + n_p \frac{I_{sc} R_{s\_0}}{R_{p\_0}} + n_p I_{0\_0} \left(\exp\left(\frac{I_{sc} R_{s\_0}}{n_p A_0 V_T} \right) - 1 \right)$$
$$= n_p \frac{R_{p\_0} + R_{s\_0}}{R_{p\_0}} I_{sc}$$
$$+ n_p I_{0\_0} \left(\exp\left(\frac{I_{sc} R_{s\_0}}{n_p A_0 V_T} \right) - 1 \right)$$

(7)

Since $n_p \frac{R_{p\_0} + R_{s\_0}}{R_{p\_0}} I_{sc} \gg n_p I_{0\_0} \left(\exp\left(\frac{I_{sc} R_{s\_0}}{n_p A_0 V_T} \right) - 1 \right)$, Equation (7) can be approximated as follows [26]:

$$n_p I_{ph\_0} \approx n_p \frac{R_{p\_0} + R_{s\_0}}{R_{p\_0}} I_{sc}$$

(8)

In an ideal case, $\frac{V_{oc}}{R_{p\_0}} \to 0$, and $I_{ph\_0} = I_{sc}$ according to Equation (4); thus, Equation (6) can be expressed as:

$$n_p I_{0\_0} = \frac{n_p I_{sc}}{\left(\exp\left(\frac{I_{sc} R_{s\_0}}{n_p A_0 V_T} \right) - 1 \right)}$$

(9)

Rearranging Equation (5) gives an expression for the shunt or parallel resistance, R_{p_0}, in the equivalent circuit as follows:

$$R_{p\_0} = \frac{\frac{n_p V_{mpp}}{n_s} + I_{mpp} R_{s\_0}}{n_p I_{ph\_0} - n_p I_{0\_0} \left(\exp\left(\frac{\frac{n_p V_{mpp}}{n_s} + I_{mpp} R_{s\_0}}{n_p A_0 V_T} \right) - 1 \right) - I_{mpp}}$$

(10)

However, the minimum and initial values of $R_{p\_0,min}$ are given as [22]:

$$R_{p\_min} = \frac{n_p}{n_s} \left(\frac{V_{mpp}}{I_{sc} - I_{mpp}} - \frac{V_{oc} - V_{mpp}}{I_{mpp}} \right)$$

(11)

The ancillary terms found in Equation (1 or 2) are defined as follows:

The thermal voltage, V_T (V), is defined as [21, 27]:

$$V_T = \frac{n_p K_B T}{q_c}$$

(12)

where K_B = Boltzmann constant (J/K), q_c= electron charge (C), T = nominal operating temperature (K).

The ideality factor in standard test condition, A_0 (-) can be expressed as [23, 24]:

$$A_0 = \frac{I_{mpp} V_{oc}}{I_{sc} V_{mpp}}; 1 \le A_0 \le 2$$

(13)

Similar to Equation (7 or 8), Equation 13 can be improved in terms of R_p and R_s for non-standard test conditions as:

$$A_0 = \frac{R_{p\_0} + R_{s\_0}}{R_{p\_0}} \frac{I_{mpp} V_{oc}}{I_{sc} V_{mpp}}; 1 \le A_0 \le 2$$

(14)

The series resistance in Equation (10) is defined as [22]:

$$R_{s\_0} = \frac{n_p}{n_s} \left(1 - \frac{I_{mpp} V_{mpp}}{I_{sc} V_{oc}} \right) \left(\frac{V_{oc}}{I_{sc}} - \frac{V_{mpp}}{I_{mpp}} \right) = \frac{n_p}{n_s} (1 - FF) \left(\frac{V_{oc}}{I_{sc}} - \frac{V_{mpp}}{I_{mpp}} \right)$$

(15)

where FF (-) is the fill-factor.

We determined the values of the following constants, I_{ph_0}, I_{0_0}, A_0, R_{p_0}, and R_{s_0} from Eqs. 7 or 8, 9, 14, 10, and 15, respectively. Then, the I-V and P-V characteristic data are generated by employing Newton-Raphson scheme as follows [27]:

$$I_m = I_{m-1} - \frac{f(I_{m-1})}{f'(I_{m-1})}$$

(16)

The function, $f(I_{m-1})$ is obtained from Equation (2) by fixing the values of the voltage, V:

$$f(I_{m-1}) = n_p I_{ph\_0} - n_p I_{0\_0} \left(\exp\left(\frac{\frac{n_p V}{n_s} + I_{m-1} R_{s\_0}}{n_p A_0 V_T} \right) - 1 \right) - \frac{\frac{n_p V}{n_s} + I_{m-1} R_{s\_0}}{R_{p_{0\_0}}} - I_{m-1} = 0$$

(17)

However, the derivative of $f(I_{m-1})$, $f'(I_{m-1})$ is obtained by differentiating Equation (17) while holding the voltage constant:

$$f'(I_{m-1}) = \frac{I_{0\_0} R_{s\_0}}{A_0 V_T} \exp\left(\frac{\frac{n_p V}{n_s} + I_{m-1} R_{s\_0}}{n_p A_0 V_T} \right) - \frac{R_{s\_0}}{R_{p_{0\_0}}} - 1$$

(18)

where m is a subscript designating the iteration.

The relative power loss, RPL (%), per module is given in Equation (19) according to Ref. [20] as follows:

$$RPL = \frac{\sum nP_{measured,cells} - \sum nP_{computed,module}}{\sum nP_{measured,cells}} \quad (19)$$

where n is the number of cells and P(W) is the power.

However, the present study defined RPL (%) as a function of Fill Factor (FF) in Equation (20):

$$RPL = \frac{FF_{measured,cells} - FF_{computed,cells}}{FF_{measured,cells}} \quad (20)$$

where the fill factor of the measured and matched series or parallel configuration [20] is expressed in Equation (21) as follows:

$$FF_{measured,cells} = \frac{\sum_{j=1}^{n} I_{mpp,j} V_{mpp,j}}{\sum_{j=1}^{n} I_{sc,j} V_{oc,j}} \quad (21)$$

However, the fill factor of computed and mismatched series and parallel module [20] is expressed in Equation (22) as follows:

$$FF_{computed,series\ module} = \frac{P_{max,series}}{I_{sc,min} \sum_{j=1}^{n} V_{oc,j}}$$
$$FF_{computed,parallel\ module} = \frac{P_{max,paraallel}}{V_{oc,max} \sum_{j=1}^{n} I_{sc,j}} \quad (22)$$

3. METHOD

3.1. The conceptual model

Five different circuit configurations of modules and arrays were considered in the search for optimum output power: series configuration (Figure 1a), parallel configuration (Figure 1b), and equal series-parallel (S=P) configuration (Figure 1c).

3.2. Input data

The input constants and variables to the computational scheme in Section 2.4. are summarized in Table 1 in Standard Test Condition (STC). The numerical values were obtained from literatures [28-31].
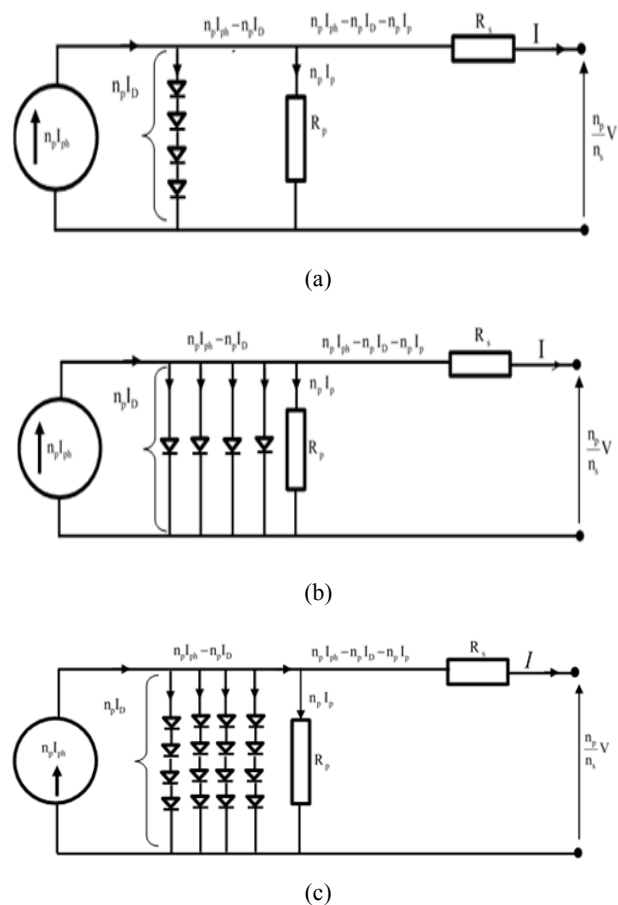

(a)

(b)

(c)

Figure 1. Equivalent circuit diagram of: (a) series configuration, (b) parallel configuration, (c) equal series-parallel configuration

Table 1. Data for different modules at AM=1.5 and G=1000 (W/m²)

S#	Constant/variable	Sym.	Unit	Value			
				MSX-60 [28]	SPSM-220D [29]	TW325P-72 [30]	ASP-400M [31]
1	Module type	-	-	MSX-60 [28]	SPSM-220D [29]	TW325P-72 [30]	ASP-400M [31]
2	Maximum output power	P_{max}	kW	0.060	0.220	0.325	0.400
3	Number of cells in series	n_s	-	36	60	72	96
4	Number of cells in parallel	n_p	-	1	1	1	1
5	Short circuit current in STC	I_{sc}	A	3.8	7.77	9.28	8.56
6	Open circuit voltage in STC	V_{oc}	V	21.1	36.24	45.60	60.00
7	Current at maximum power point	I_{mpp}	A	3.5	7.35	8.75	8.04
8	Voltage at maximum power point	V_{mpp}	V	17.1	29.94	37.10	49.08
9	Temperature coefficient of short circuit current	k_i	%/K	0.065	0.040	0.041	0.037
10	Temperature coefficient of open circuit voltage	k_v	%/mV	-80	-30	-31	-24
11	Temperature at STC	T_0	K	298.15	298.15	298.15	298.15
12	Irradiance at STC	G_0	W/m²	1000	1000	1000	1000
13	Boltzmann constant	K_B	J/K	1.381×10^{-23}	1.381×10^{-23}	1.381×10^{-23}	1.381×10^{-23}
14	Electron charge	q_c	C	1.6×10^{-19}	1.6×10^{-19}	1.6×10^{-19}	1.6×10^{-19}
15	Energy gap for c-Si	E_g	eV	1.11	1.11	1.11	1.11
16	Ideality factor in STC	A_0	–	1.13994	1.14709	1.16155	1.13378
17	Parallel resistance in STC (min.)	$R_{p0,min}$	Ω	1.55159	1.17381	2.50609	0.98438
18	Series resistance at STC (min.)	R_{s0}	Ω	0.00470	0.00215	0.00218	0.00187

19	Diode saturation or reverse current	I_{0_0}	A	7.94727×10^{-09}	1.00385×10^{-08}	5.7959×10^{-09}	4.23354×10^{-09}
20	Photon or light current	I_{ph0}	A	3.81150	7.78424	9.30109	8.57628
21	Fill factor	FF	–	0.748	0.781	0.768	0.779

3.3. Computational scheme

The computational scheme in Figure 2 gives the logical flow and the strategic design of the analysis in order to address the key objectives of this work. At a glance, Figure 2 indicates three drops at the first summing point. Thus, three analytic routes are created for series, parallel, and series-parallel configurations, whereas the second summing point indicates the module or array type, which could be either a matched or mismatched configuration. The matched module or array consists of panels of homogeneous electrical and thermophysical properties, whereas the matched module or array consists of panels of heterogeneous electrical and thermophysical properties.
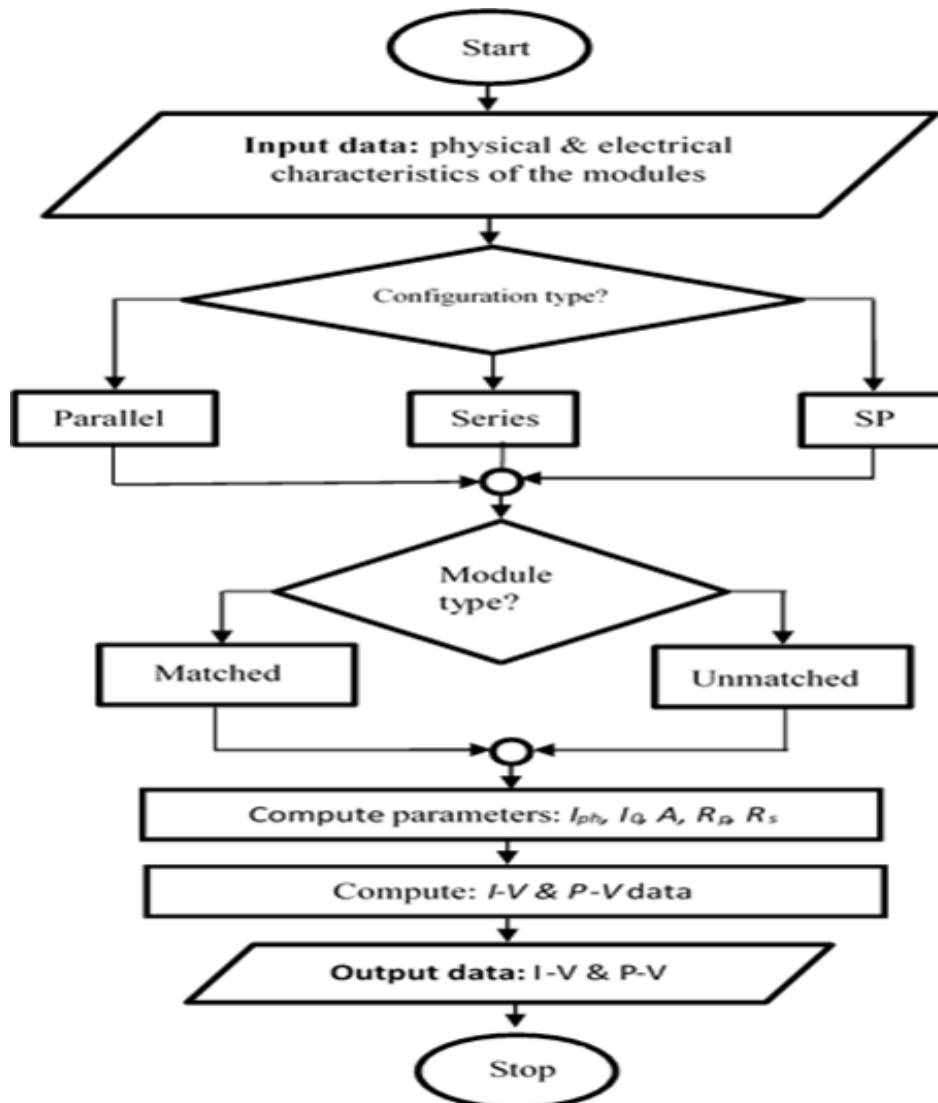

Figure 2. Flow chart for array configuration and computation of RPL

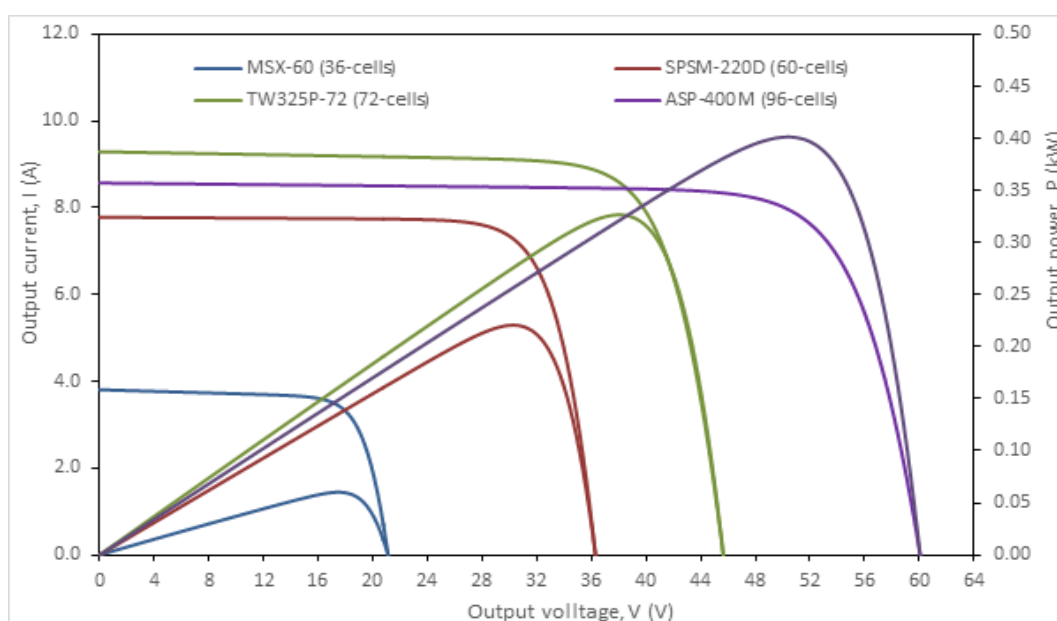## 4. RESULTS AND DISCUSSION

4.1. Result presentation

Table 2 shows the estimated values $\{I_{ph}, I_0, A, R_p, R_s\}$ for the five-parameter model, which is capable of driving the simulated output power very close to the measured output power in the standard test condition with a negligible difference between the computed and measured output power. These sets of constants were substituted into Eqs. 16-18 to obtain the I-V and P-V curves for the four selected demonstration modules (MSX-60, SPSM-220D, TW325P-72,

ASP-400M). The I-V and P-V curves for the demonstration modules are shown in Figure 3. Moreover, the measured output power rates in Table 1 (and simulated output power in Table 2) for the modules, MSX-60, SPSM-220D, TW325P-72, ASP-400M are 0.05985 (0.06003), 0.22006 (0.22045), 0.32463 (0.32659), 0.39460 (0.40137) kW were respectively in good agreement, which indicates that the equivalent circuit parameters were aptly determined. Thus, these results validate the authenticity of the proposed equivalent circuit models presented in Eqs. 1-18.

Table 2. The computed model parameters for the selected modules in standard test condition (25 °C, AM=1.5 and 1 kW/m²)

| Parameter	Symbol	Unit	Computed value			
			MSX-60	SPSM-220D	TW325P-72	ASP-400M
Number of cells	n	-	36	60	72	96
Photon current	I_{ph}	A	3.81150	7.78424	9.30109	8.57628
Diode reverse or saturation current	I_0	A	7.94727×10^{-09}	1.00385×10^{-08}	5.7959×10^{-09}	4.23354×10^{-09}
Ideality factor	A	—	1.14339517	1.1491926	1.16418801	1.13593746
Shunt or parallel resistance	R_p	Ω	3.04991945	9.19608693	2.50609225	3.31810158
Series resistance	R_s	Ω	0.00479001	0.00214437	0.00218206	0.00188495
Maximum output power	P_{max}	kW	0.06003	0.22045	0.32659	0.40137

Figure 3. I-V and P-V curves for the individual demonstration modules

4.2. Discussion of results

For number of cells, n, ranging from 36 to 96, the maximum output power, which is the key performance yardstick, increased with increasing number of cells; however, for n>96, the efficiency of the module decreased [14], which could be attributed to open circuit defect losses due to predominance of series configuration. Thus, modules with a high number of cells (n > 96) should not be used in setting up a PV plant as inevitable open circuit losses will favor mismatch losses in such modules. This is in agreement with the thermodynamic principle, which asserts that the efficiency of a system decreases as the number of components increases; thus, the modules with the number of cells above 96 cells were not included in the analysis in order the results clean and unflawed.

  Figures 4 (a-d) and Figure 4e show the I-V and P-V curves for the four matched and mismatched modules in series configuration with the same and different electrical and thermal characteristics, respectively. The behavior of these curves is identical to those of weak and strong cells connected in series [20]. The weak cell dictates the magnitude of current, but the voltage cumulatively builds up. The module with the smallest number of cells (MSX-60) dominated the value of

current, although the voltage tends to increase as the modules of the large number of cells were added [9]. From Figure 4e, the maximum output power of four mismatched modules (MSX-60 + SPSM-220D + TW325P-72 + ASP-400M) gave 0.4644 kW , but those of the four matched modules of MSX-60, SPSM-220D, TW325P-72, and ASP-400M gave maximum output power rates of 0.2406, 0.8825, 1.3065, and 1.6057 (kW), respectively. Apparently, the relative power loss was determined when comparing the power obtained from the matched to mismatched modules for the S configuration mentioned in the objective. The output power of the matched modules (MSX-60) was less than that of the mismatched modules, implying that the total number of cells in those matched modules was less than that of cells in the mismatched modules for modules (SPSM-220D, TW325P-72 and ASP-400M), and vice versa. Thus, once there are a commensurate number of cells (non-redundancy), the effect of power loss in matched and mismatched modules can be accurately determined. Thus, a common number of cells need to be observed before establishing the Real RPL (RRPL) which is the reason why the present work adopted the fill factor in computing RRPL.
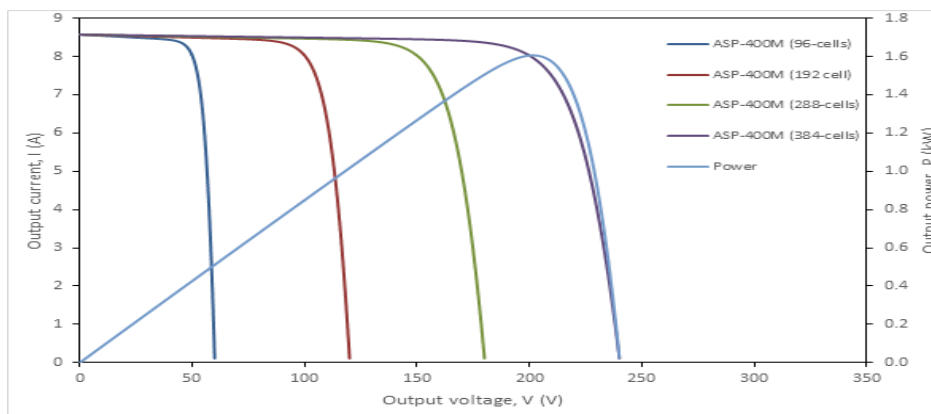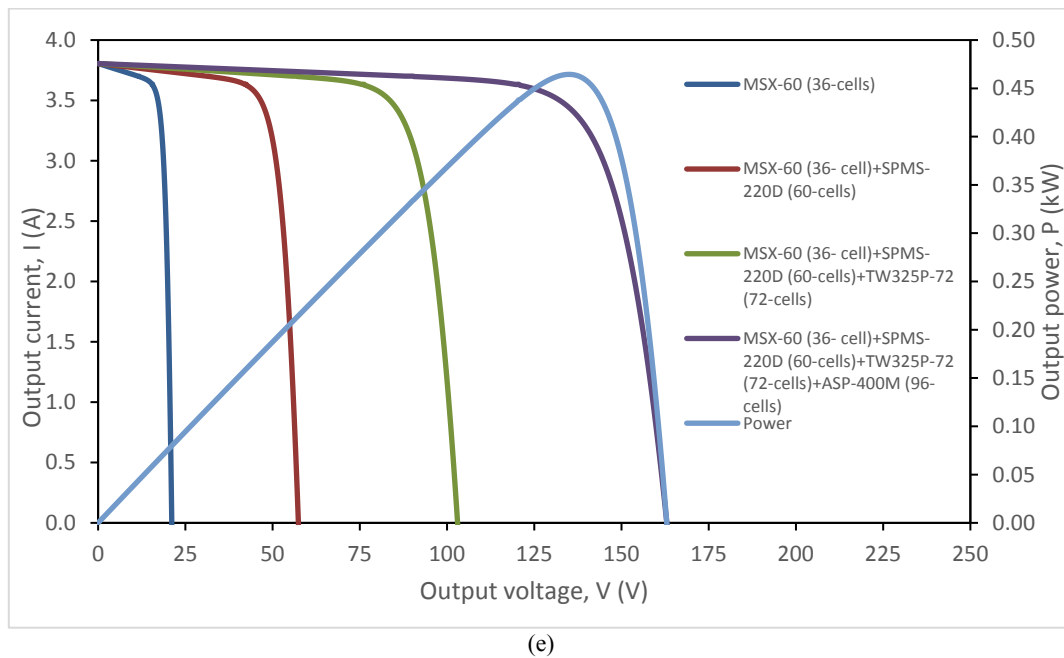
(a)

(b)

(c)

(d)

(e)
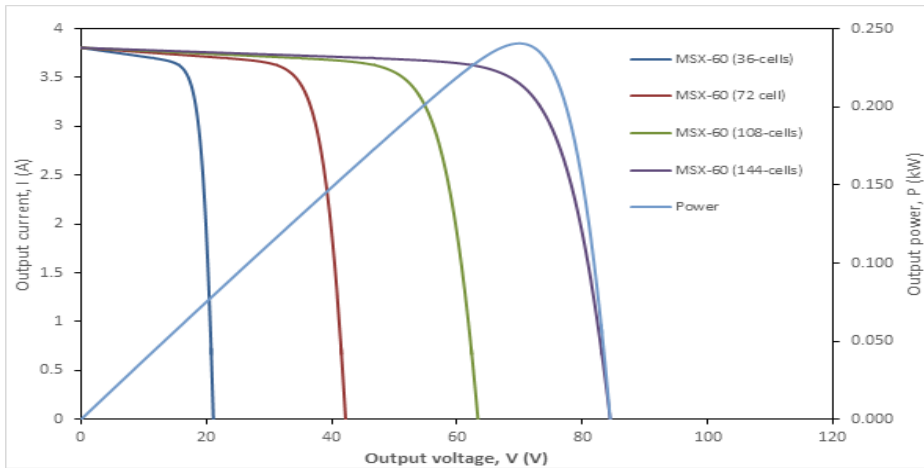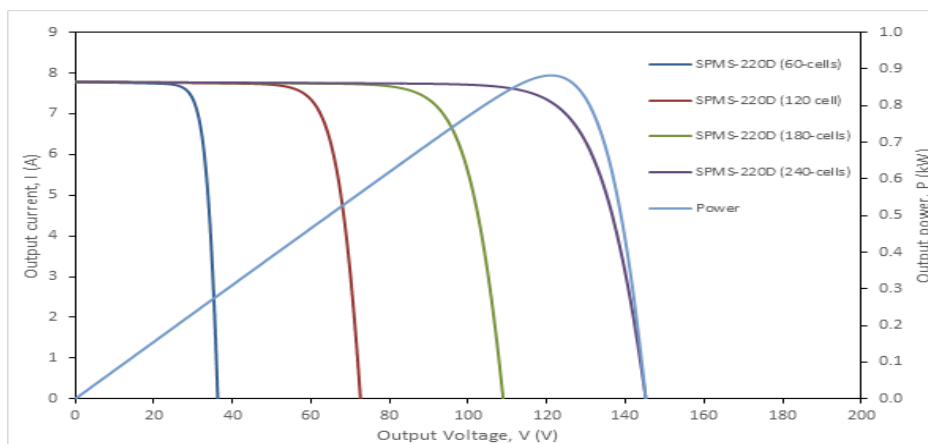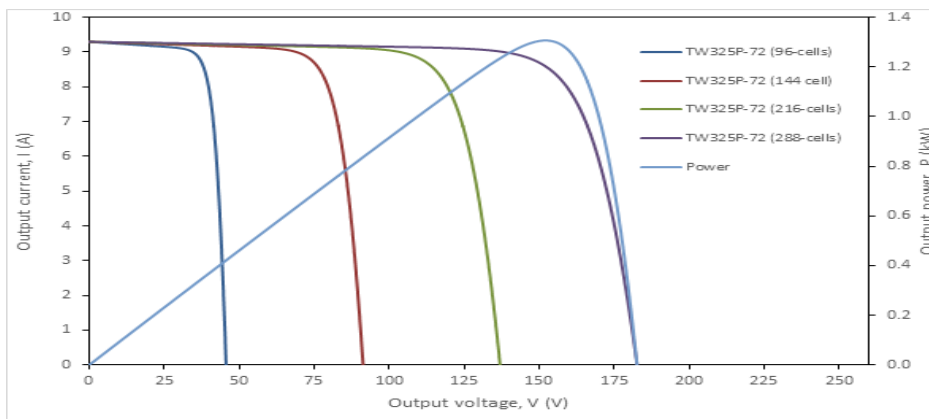
Figure 4. I-V and P-V curves for the matched: (a) MSX-60 series(S) configuration, (b) SPMS-220D series(S) configuration, (c) TW325P-72 series(S) configuration, (d) ASP-400M series(S) configuration and (e) I-V and P-V curves for the mismatched series(S) configuration

Quantitatively, the four matched modules of SPSM-220D, TW325P-72, and ASP-400M gave higher maximum output power than those of four mismatched modules (MSX-60 + SPSM-220D + TW325P-72 + ASP-400M) at excess values of 0.4181, 0.8421 and 1.1413 (kW), respectively. Apparently, there is no advantage to combining mismatched modules with different electrical and thermal characteristics in series configuration. It simply amounts to a substantial power loss in mismatched array and should be avoided by designers and

installers of PV modules. Also, Table 3 supports that more RPL is associated with mismatched modules, whereas close to zero RPL is associated with the technologies of matched modules [20]. Moreover, power losses due to defects in the open circuit voltage are significant in mismatched modules. In order to avert the problem of RPL in the series configuration, the present work recommends the application of matched modules as a palliative measure.
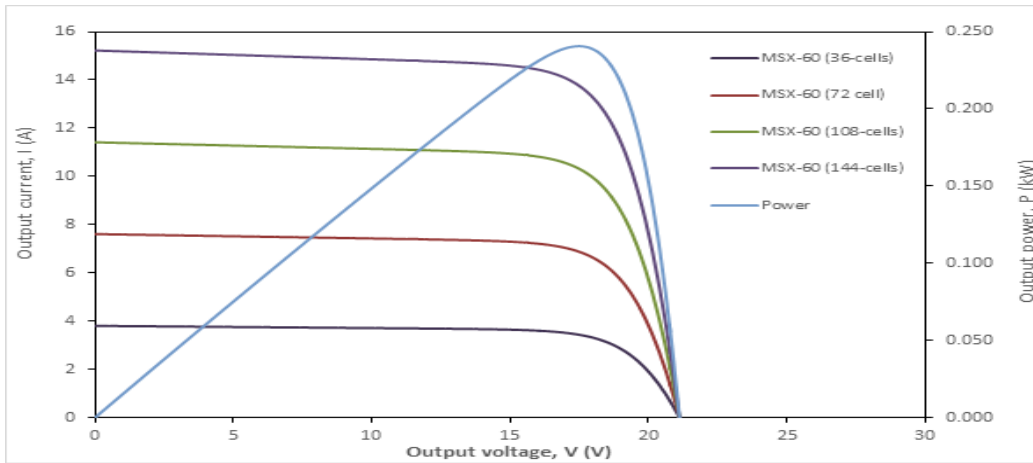
Table 3. Relative power loss in series configuration

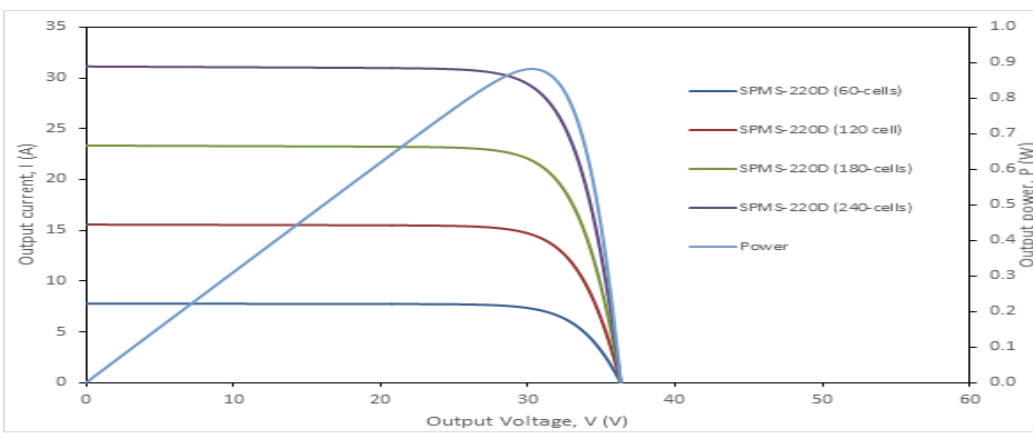| S#	Module	Characteristic	n_cell	Power, P (kW)	Measured Fill factor, $FF_{measured}$	Computed Fill factor, $FF_{computed}$	RPL (%)	Figure
1	MSX-60	Matched (4)	144	0.2406	0.75	0.75	0.0	4a
2	SPSM-220D	Matched (4)	240	0.8825	0.78	0.78	0.0	4b
3	TW325P-72	Matched (4)	288	1.3065	0.77	0.77	0.0	4c
4	ASP-400M	Matched (4)	384	1.6057	0.78	0.78	0.0	4d
5	All	Mismatched (4)	264	0.4644	0.77	0.75	2.6	4e

Figures 5 (a-d) and Figure 5e show the I-V and P-V curves for the four matched and mismatched modules in a parallel configuration, respectively. The former and latter modules have the same and different electrical and thermal characteristics, respectively. The behaviors of these curves are akin to those of weak and strong cell connection in parallel configuration. The stronger module dictates the magnitude of the voltage applied, but the current cumulatively builds up. Therefore, the module with the highest number of cells (ASP-400M) dominates the output voltage, although the output current tends to increase as the modules of the lower number of cells were added [19], whereas Figure 5e gives the maximum output power of the four mismatched modules (MSX-60 + SPSM-220D + TW325P-72 + ASP-400M) as 1.370 kW, but those of the four matched modules (MSX-60, SPSM-220D, TW325P-72 and ASP-400M) in Figures 5 (a-d) gave maximum output power of 0.24060, 0.88255, 1.3065 and 1.6057 kW, respectively.

However, having four mismatched modules of MSX-60, SPSM-220D, TW325P-72, and ASP-400M in parallel

configuration gave much maximum output power (1.370 kW) compared to those of series configuration (0.4644 kW). Consequently, the RPL in parallel configuration was suppressed to 1.2 % in Table 5, since the maximum output of the mismatched parallel configuration is higher than that of the series counterpart in Table 4, but the RPL was enhanced to 2.6 %. This phenomenon simply buttresses the fact that the parallel configuration remains more resistant to short circuit defects. However, the influence of short circuit defects becomes significant, and this could be suppressed by introducing power electronics device (the MPPT tracker) or DC-DC or micro-inverter to minimize RPL in parallel configuration [19]. Therefore, parallel configuration is superior to series configuration in case of mismatch in technological configuration [4]. This observation becomes obvious if the equivalent circuit model analysis is carried out at normalized or optimum shunt resistance; otherwise, the RPL cannot be trivial if the shunt resistance approaches infinity as the maximum output power is being reduced [20].
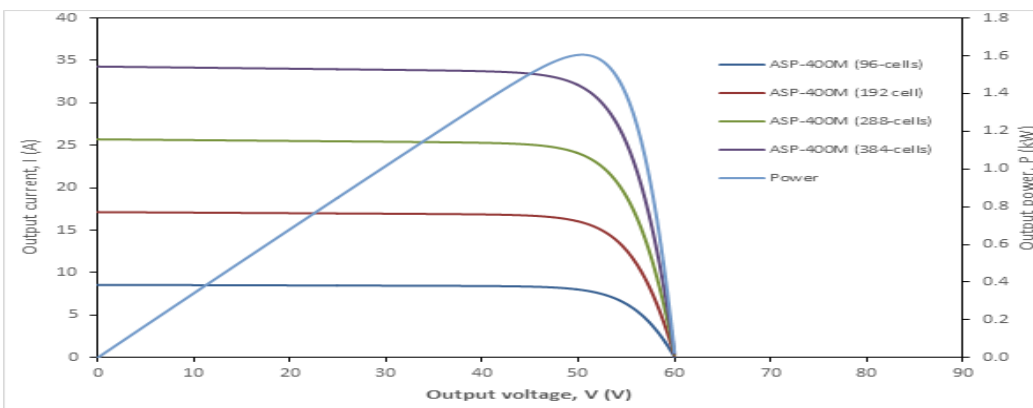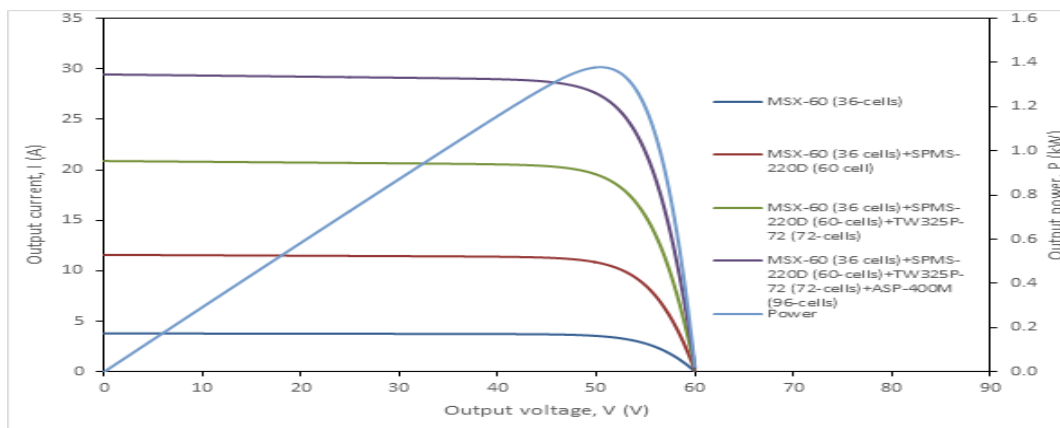
(a)

(b)
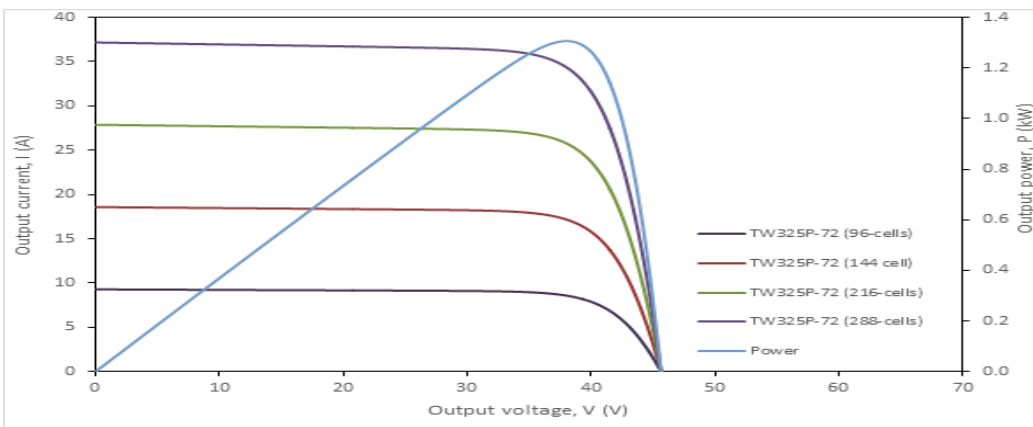
(c)

(d)

(e)

Figure 5. I-V and P-V curves for the matched: (a) MSX-60 parallel (P) configuration, (b) SPMS-220D parallel (P) configuration, (c) TW325P-72 parallel (P) configuration, (d) ASP-400M parallel (P) configuration and (e) I-V and P-V curves for the mismatched parallel (P) configuration

Table 4. Relative power loss in parallel configuration

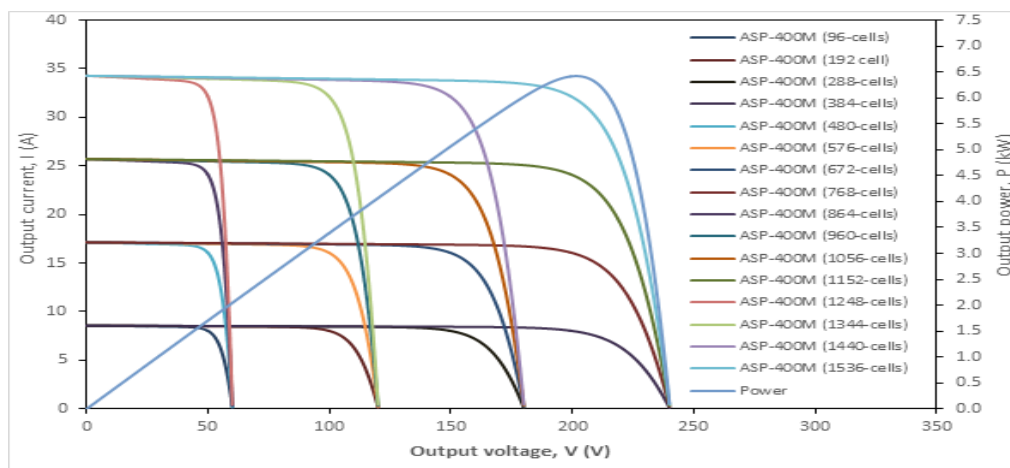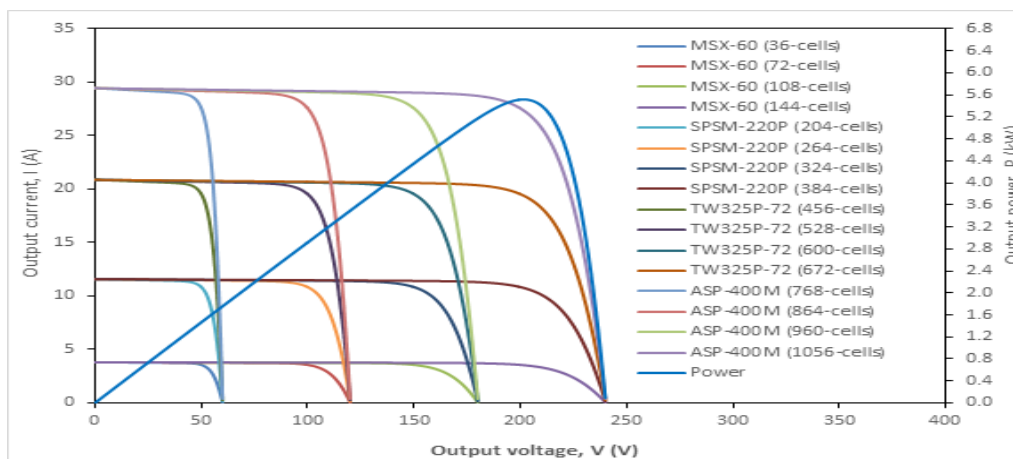| S#	Module	Characteristic	n_cell	Power, $P_{computed}$ (kW)	Measured Fill factor, $FF_{measured}$	Computed Fill factor, $FF_{computed}$	RPL (%)	Figure
1	MSX-60	Matched (4)	144	0.2406	0.75	0.75	0.0	5a
2	SPSM-220D	Matched (4)	240	0.8825	0.78	0.78	0.0	5b
3	TW325P-72	Matched (4)	288	1.3065	0.77	0.77	0.0	5c
4	ASP-400M	Matched (4)	384	1.6057	0.78	0.78	0.0	5d
5	All	Mismatched (4)	264	1.3700	0.77	0.76	1.3	5e
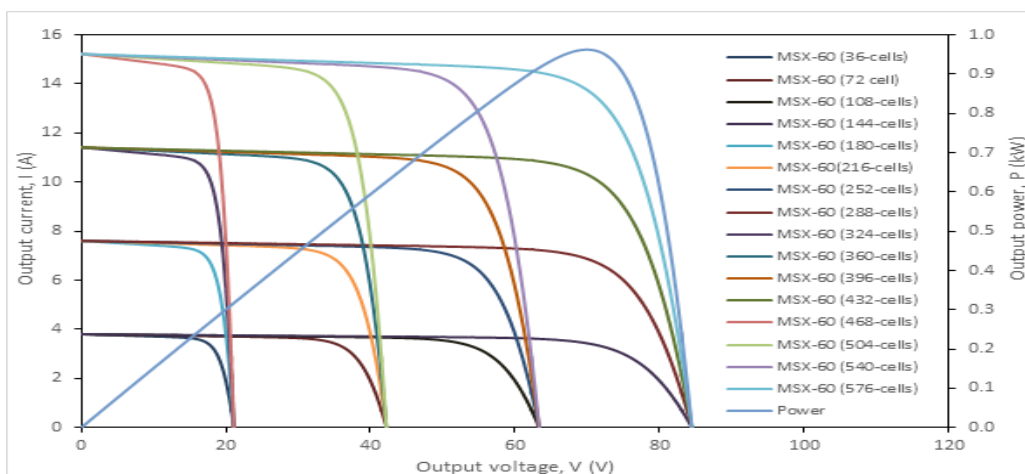
(a)
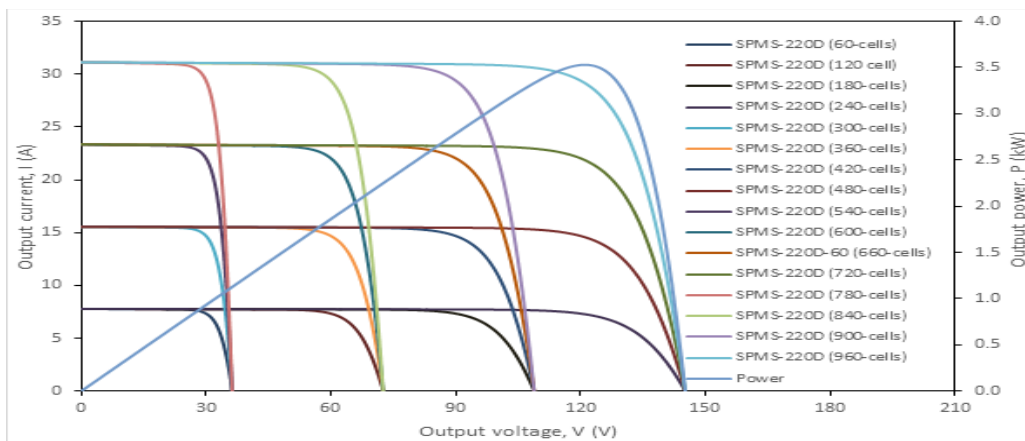
(b)
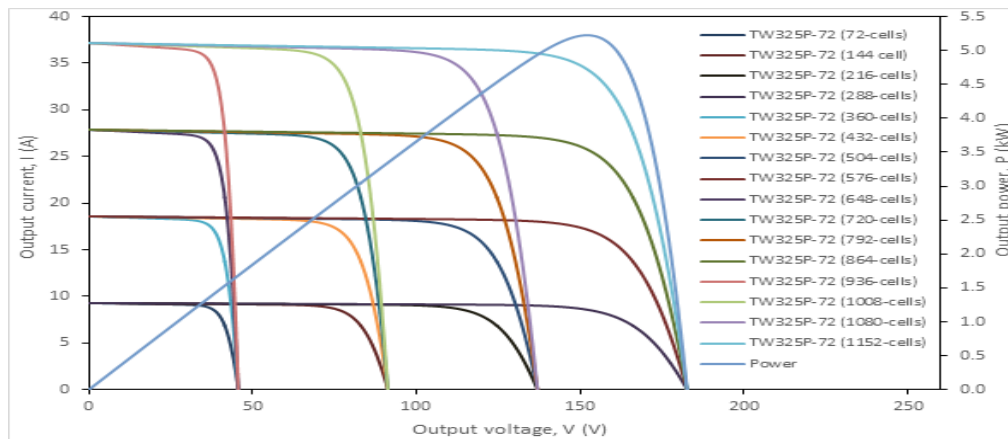
(c)

(d)

(e)

Figure 6. I-V and P-V curves for the: (a) MSX-60 matched array, (b) SPMS-220D matched array, (c) TW325P-72 matched array, (d) ASP-400M matched array and (e) I-V and P-V curves for the mismatched array

Figures 6 (a-d) present the maximum output power of equal series-parallel configuration of sixteen matched modules (MSX-60, SPSM-220D, TW325P-72, ASP-400M) which gave maximum output power rates of 0.9625, 3.5301, 5.2260, 6.4229 kW, respectively, but those of sixteen mismatched modules (MSX-60 + SPSM-220D + TW325P-72 + ASP-400M) in Figure 6e gave 5.5169 kW in Table 5. Notably, the characteristics of series-parallel array are similar to those of parallel modules, sequel to the four strings (or blocks) responsible for lowering RPL to 1.3 %, as reported in Tables 4 and 5. Thus, increasing the number of strings minimizes the

inherent RPL in an array. Also, the matched technology in Tables 3-5 showed a trivial RPL, which implies that the total output power of the cells is approximately equal to that of the module. This indicates that the electrical and thermal properties of the cells and the modules are in alignment. Hence, designers and installers of photovoltaic plants should adhere to use of modules or arrays of matched or uniform electrical and thermal properties to enhance output power.

Moreover, by comparing the RPL of mismatched technologies in Tables 3 and 4 (or 5), the RPL associated with the series configuration (2.6 %) is twice that of the parallel

configuration (1.3 %) and these results are in agreement with those of Vicente et al. [20]. This implies that open circuit defect is more pronounced in series configuration and more than a short circuit defect in parallel configuration. This could be remedied by simply increasing the number of blocks or strings in the design of photovoltaic arrays or by avoiding the use of mismatched modules in the design of photovoltaic plants.

Table 5. Relative power loss in series-parallel configuration in Figure 1c

S#	Module	Characteristic	n_cell	Power, $P_{computed}$ (kW)	Measured Fill factor, $FF_{measured}$	Computed Fill factor, $FF_{computed}$	RPL (%)	Figure
1	MSX-60	Matched (16)	576	0.9625	0.75	0.75	0.0	6a
2	SPSM-220D	Matched (16)	960	3.5301	0.78	0.78	0.0	6b
3	TW325P-72	Matched (16)	1152	5.2260	0.77	0.77	0.0	6c
4	ASP-400M	Matched (16)	1536	6.4229	0.78	0.78	0.0	6d
5	All	Mismatched (16)	1056	5.5169	0.77	0.76	1.3	6e

5. CONCLUSIONS

A configuration analysis of the modules and arrays was successfully carried out via real equivalent circuit model for matching and mismatched: series (S), parallel (P), and series-parallel (SP) configurations in standard test conditions. Comparison of the maximum output power for the first two configurations showed that for the equal number of mismatched modules, the parallel configuration (P) was superior to series configuration (S) due to less RPL associated with the parallel configuration. Moreover, parallel configuration (P) had a greater tendency to resist inhomogeneity in electrical and thermal characteristics of modules, leading to relative power losses in an array. However, there was no discrepancy in the maximum output power for different matched configurations (S and P). The relative power loss was more recurrent in mismatched series configuration due to open circuit defect. Thus, the application of mismatched modules with heterogeneous electrical and thermal characteristics should be avoided in order to minimize power losses in modules or arrays. Pertinently, the present work suggests the application of power electronics device as a means of curbing the RPL in parallel configuration and the application of integral bypass diode as a means of minimizing the RPL in series configuration. Furthermore, mismatched modules should be avoided when designing and installing photovoltaic power plants to enhance power generation from power plants.

6. ACKNOWLEDGEMENT

NOMENCLATURE

A	Ideality factor
AM	Air mas
BL	Bridge-linked interconnection
DC	Direct curren
FF	Fill-factor
HC	Honeycomb interconnection
I	Current
I-V	Current-voltage
K	Boltzmann constant
LAD	Ladder interconnection
MPPT	Maximum power point tracking
NOC	Nominal operating cell temperature
OC	Open circuit
P	Parallel configuration
PTC	PVUSA test condition
P-V	Power-voltage
PVUSA	Photovoltaic USA
R	Resistance
RPL	Relative power losses
RRPL	Real relative power losses
S	Series configuration
SC	Short circuit
SP	Series-parallel configuration
STC	Standard test condition
T	Cell operating temperature
TCT	Total-cross-tied interconnection
V	Voltage

REFERENCES

1. Balram, G., Anitha, S. and Deshmukh, A., "Utilization of renewable energy sources in generation and distribution optimization", *Proceedings of the International IOP Conference Series: Material Science Engineering, Vol. 981, International Confetrence on Recent Advancements in Engineering and Management (ICRAEM-2020)*, Warangal, India, (October 9-10, 2020), 042054. (https://doi.org/10.1088/1757-899X/981/4/042054).

2. Williams, B.K. and Nichols, J.D., "Optimization in natural resources conservation", In: Guntenspergen, G., Eds, Application of threshold concepts in natural resource decision making, Springer, New York, NY, (2014), 45-65. (https://doi.org/10.1007/978-1-4899-8041-0_4).

3. Marodkar, M.M., "Study of pv array configuration and its effects on performance under nonuniform irradiance", *Proceedings of International Conference on Electrical, Electronics, Signals, Communication and Optimization (EESCO)*, Visakhapatnam, India, (Jan. 24-25, 2015), 1-5. (https://doi.org/10.1109/EESCO.2015.7253902).

4. Burhanudin, K., Kamarzaman, N.A., Samat, A.A.A., Tajudin, A.I., Ramli, S.S. and Hidayat, N., "An improved photovoltaic array configuration for photovoltaic system in the presence of maximum power point tracking during partial shading condition", *Indonesian Journal of Electrical Engineering and Computer Science*, Vol. 6, No. 2, (2017), 301-309. (http://doi.org/10.11591/ijeecs.v6.i2.pp301-309).

5. Fan, Q., An, Q., Lin, Y., Xia, Y., Li, Q., Zang, M., Su, W., Peng, W., Zang, C., Liu, F., Hou, L., Zhu, W., Yu, D., Xiano, M., Moon, E., Zang, F., Anthopoulos, T.D., Linganas, O. and Wang, E., "Over 14 % efficiency all-polymer solar cells enabled by a low bandgap polymer acceptor with low energy loss and efficient charge separation", *Energy & Environment Science*, Vol. 13, No. 12, (2020), 1-27. (https://doi.org/10.1039/D0EE01828G).

6. Chikate, B.V. and Sadawarte, Y.A., "The factors affecting the performance of solar cell", *International Journal of Computer Applications, Proceedings on International Conference on Advancements in Engineering and Technology (ICAET 2015), (ICQUEST 2015)*, No. 1, (2015), 4-8. (https://www.https://www.ijcaonline.org/proceedings/icquest2015/number1/22976-2776).

7. Srinivasan, A., Devakirubakaran, S. and Sundaram, B.M., "Mitigation of mismatch losses in solar pv system–two-step reconfiguration approach", *Solar Energy*, Vol. 206, (2020), 640-654. (https://doi.org/10.1016/j.solener.2020.06.004).

8. Mahmoud, Y. and El-Saadany, E.F., "Enhanced reconfiguration method for reducing mismatch method for reducing mismatch", *IEEE Journal of Photovoltaics*, Vol. 99, (2017), 1-9. (https://doi.org/10.1109/JPHOTOV.2017.2752708).

9. Bonthagorla P.K and Mikkili S., "Performance analysis of PV array configurations (SP, BL, HC and TT) to enhance maximum power under

non-uniform shading conditions", *Engineering Reports*, Vol. 2, (2020), e12214. (https://doi.org/10.1002/eng2.12214).

10. Mohammadnejad, S., Khalafi, A. and Ahmadi S.M., "Mathematical analysis of total-cross-tied photovoltaic array under partial shading condition and its comparison with other configurations", *Solar Energy*, Vol. 133, (2016), 501-511. (https://doi.org/10.1016/j.solener.2016.03.058).

11. Christabel, S.C., Srinivasan, A., Winston, D.P. and Kumar, B.P., "Reconfiguration solution for extracting maximum power in the aged solar pv systems", *Journal of Electrical Engineering*, Vol. 16, No. 3, (2016), 440-446. (https://www.researchgate.net/publication/319502192_Reconfiguration_solution_for_extracting_maximum_power_in_the_aged_solar_PV_syste ms).

12. Renogy, R., "Learn series and parallel", (2017). (https://www.renogy.com/learn-series-and-parallel/), (Accessed: 07 October 2017).

13. Fei, L., Guo, S., Walsh, T.M. and Aberle, G.A., "Improved pv module performance under partial shading condition", *Energy Procedia*, Vol. 33, (2013), 248-255. (https://doi.org/10.1016/j.egypro.2013.05.065).

14. Pendem S.R. and Mikkili S., "Modeling, simulation and performance analysis of solar pv array configurations (series, series–parallel and honey-comb) to extract maximum power under partial shading conditions", *Energy Reports*, Vol. 4, (2018), 274-287. (https://doi.org/10.1016/j.egyr.2018.03.003).

15. Ferahtia, S., Djerioui, A., Zeghlache, S. and Houari, A., "A hybrid power system based on fuel cell, photovoltaic source and supercapacitor", *SN Applied Science* Vol. 2, No. 940, (2020). (https://doi.org/10.1007/s42452-020-2709-0).

16. Nguyen, X.H. and Nguyen, M.P., "Mathematical modeling of photovoltaic cell/module/arrays with tags in MATLAB/SIMULINK", *Environmental Systems Research*, Vol. 4, (2015), 24. (https://doi.org/10.1186/s40068-015-0047-9).

17. Salem, F.A., Matrawy, K.K. and Mahrous, A.F., "Mathematical modeling of PV array with different performance parameters", *International Journal of Control, Automation and Systems*, Vol. 4, No. 2, (2015). (http://www.researchpub.org/journal/jac/jac.html).

18. Vicente, P.D., Pimenta, T.C. and Ribeiro, E.R., "Photovoltaic array reconfiguration strategy for maximization of energy production", *International Journal of Photoenergy*, Vol. 11, (2015), 592383. (http://doi.org/10.1155/2015/592383).

19. Fornie´s, E., Naranjo, F., Mazo, M. and Ruiz, F. "The influence of mismatch of solar cells on relative power loss of photovoltaic modules", *Solar Energy*, Vol. 97, No. 2, (2013), 39-47. (https://doi.org/10.1016/j.solener.2013.08.004).

20. Nnamchi, S.N., Mundu, M.M., Busingye, J.D. and Ezenwankwo, J.U., "Extrinsic modeling and simulation of helio-photovoltaic system: A case of single diode model", *International Journal of Green Energy*, Vol. 16, No. 6, (2019), 450-467. (https://doi.org/10.1080/15435075.2019.1578659).

21. Nnamchi, S.N. and Nnamchi, O.A., "Perturbation of diminutive solar irradiance and extreme semiconductor temperature on the output current and voltage: The translation of electrical characteristics into thermal characteristics", *Journal of Solar Energy Research*, Vol. 4, No. 2, (2019b). 92-106. (https://doi.org/10.1080/15435075.2019.1578659).

22. Yahyaoui, I., Specifications of photovoltaic pumping systems in agriculture: Sizing, fuzzy energy management and economic sensitivity analysis, Elsevier, (2016), 121-133. (https://www.elsevier.com/books/specifications-of-photovoltaic-pumping-systems-in-agriculture/yahyaoui/978-0-12-812039-2).

23. Ahmad, T., Sobhan, S. and Nayan, M.F., "Comparative analysis between single diode and double diode model of PV cell, concentrate different parameters effect on its efficiency", *Journal of Power and Energy Engineering*, Vol. 4, (2016), 31-46. (https://doi.org/10.4236/jpee.2016.43004).

24. Baba, A.O., Liu, G. and Chen, X., "Classification and evaluation review of maximum power point tracking methods", *Sustainable Futures*, Vol. 2, (2020), 100020. (https://doi.org/10.1016/j.sftr.2020.100020).

25. Hayt, W.H., Kemmerly, J.E. and Durbin, S.M., Engineering circuit analysis, 9th Ed., McGraw-Hill, New York, (2020). (https://www.aldeatdo.com/wp-content/uploads/2019/09/William_Hart_Hayt_Jack_E_Kemmerly_Steve n_M_Durbz-lib.org_.pdf).

26. Belkassmi,Y., Rafiki, A., Gueraoui, K., Bonkoungou, D., Koalaga, Z. and Njomo, D., "Modeling and simulation of photovoltaic module based on one diode model using MATLAB/SIMULINK ", *Proceedings of International Conference on Engineering & MIS (ICEMIS)*, Monastir, Tunisia, (2017). (https://doi.org/10.1109/icemis.2017.8272965).

27. Nnamchi, S.N., Nnamchi, A.O., Sanya, O.D., Mundu, M.M. and Gabriel, V., "Dynamic analysis of performance of photovoltaic generators under moving cloud conditions", *Journal of Solar Energy. Research*, Vol. 5, No. 2, (2020), 453-468. (https://doi.org/10.22059/jser.2020.304561.1158).

28. Solarex D., "Msx-60 and msx-64 photovoltaic module", (2020). (https://www.solarelectricsupply.com), (Accessed: 12 August 2017).

29. Shangpin S.D., "Poly-crystalline solar module spsm-22", (2020). (http://www.wxsunpower.com/images/new/new05.jpg), (Accessed: 15 August 2017).

30. Tongwei S.D., "Specifications of tw305p-72 polycrystalline solar module", (http://www.tw-solar.com/en/Uploads/2014/0124/256bf277.pdf.), (Accessed: 16 August 2020).

31. Manufacturer, D.S., "Advanced solar photonics asp-400m solar", (http://www.solardesigntool.com/components/module-panel-solar/Advanced-Solar-Photonics/1737/ASP-400M/specification-data-sheet.html), (Accessed 17 August 2020).